ACS APPLIED MATERIALS & INTERFACES

Research Article

www.acsami.org

Salicylic Acid As a Tridentate Anchoring Group for *azo*-Bridged Zinc Porphyrin in Dye-Sensitized Solar Cells

Faliang Gou,[†] Xu Jiang,[†] Bo Li,[†] Huanwang Jing,*[,†,‡] and Zhenping Zhu[‡]

[†]State Key Laboratory of Applied Organic Chemistry, College of Chemistry and Chemical Engineering, Lanzhou University, Lanzhou, Gansu 730000, China

[‡]State Key Laboratory of Coal Conversion, Institute of Coal Chemistry, Chinese Academy of Sciences, Taiyuan, Shanxi 030001, China

Supporting Information

ABSTRACT: Two series dyes of *azo*-bridged zinc porphyrins have been devised, synthesized, and performed in dye-sensitized solar cells, in which salicylic acids and *azo* groups were introduced as a new anchoring group and π-conjugated bridge *via* a simple synthetic procedure. The representation of the new dyes has been investigated by optical, photovoltaic, and electrochemical means. The photoelectric conversion efficiency of their DSSC devices has been improved compared with other DSSC devices sensitized by symmetrical porphyrin dyes. The results revealed that tridentate binding modes between salicylic acid and TiO_2 nanoparticles could enhance the efficiency of electron injection. The binding modes between salicylic acid and TiO_2 nanoparticles may play a crucial role in the photovoltaic performance of DSSCs.

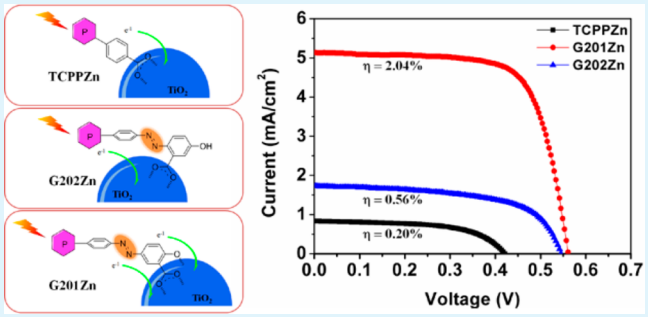

KEYWORDS: *dye-sensitized solar cells, salicylic acid, anchoring group, azo-bridge, porphyrin dye*

INTRODUCTION

As an alternative energy technology, dye-sensitized solar cells have received extensive attention owing to their low costs and good photoelectric conversion efficiency.[1−4] The DSSC of polypyridyl ruthenium complexes produced an efficiency of photoelectric conversion up to 11% under standard global AM 1.5 solar conditions.[5−7] However, there are still several drawbacks, such as resource scarcity, high costs, and environmental issues which would limit their industrial applications. Metalloporphyrins[8−11] are the optimal choices because they have intense absorbing Soret bands and moderate absorbing Q bands and their rigid molecular structures are favorable to the transportation of electrons. Some porphyrin dyes, such as YD and LD series,[8,12−15] with the anchoring group of 4-ethynylbenzoic acid attached at the *meso* position have displayed better energy conversion efficiency (12.3%),[16] but these dyes entail complicated syntheses, which would limit their applications. The symmetrical porphyrin dyes[9,10] are relatively easy to be synthesized in spite of their lower efficiency of photoelectric conversion. A typical porphyrin dye with four benzoic acids as anchoring groups was reported by Rochford et al.[17] The photovoltaic performance of this type of dye could be enhanced by the formation of blocking layers.[18]

The majority of sensitizers are linked to the TiO_2 semiconductor through carboxyl groups as anchoring groups, which provide a good electron injection to the conducting band of semiconductor. The binding mode of an anchoring group is considered an important factor to upgrade the performance of DSSC devices. Generally, the carboxyl is a standard anchoring group for sensitizers providing three binding modes between the TiO_2 surface and the dye.[19−21] Recently, some researchers made efforts to developing novel anchoring groups that would enhance the photoelectric efficiency. For example, catechol was used as an anchoring group for Cat dyes;[22] 8-hydroxylquinoline was reported as an anchoring group for metalloporphyrin-sensitized solar cells;[23] perylene anhydride was fused on porphyrin dyes for this device;[24] pyridine ring was also reported as an anchoring group by Ooyama et al.[25] Tian et al. reported that 2-(1,1-dicyanomethylene) rhodanine is an alternative anchoring group for organic sensitizers.[26] Sun et al.[27] reported the hydroxyl group connecting a dye to the surface of nano-TiO_2 that guarantees efficiently electron-injection and regeneration.

Focusing on this new strategy discovering novel anchoring group, we designed and synthesized two series *azo*-bridged zinc porphyin dyes. The carboxyl and hydroxyl as anchoring groups were introduced into the dyes of G201Zn and G202Zn (Figure 1) through a simple coupling reaction of 5,10,15,20-*tetra*-(*p*-amminophenyl) porphyrin (TAPP) and hydroxyl benzoic acid (Figure 2). The nitrogen−nitrogen double bonds of *azo* groups were constructed as bridges in the meantime, which have been primarily used in organic dyes by Mikroyannidis et al.[28] To

Received: September 14, 2013
Accepted: November 14, 2013
Published: November 14, 2013

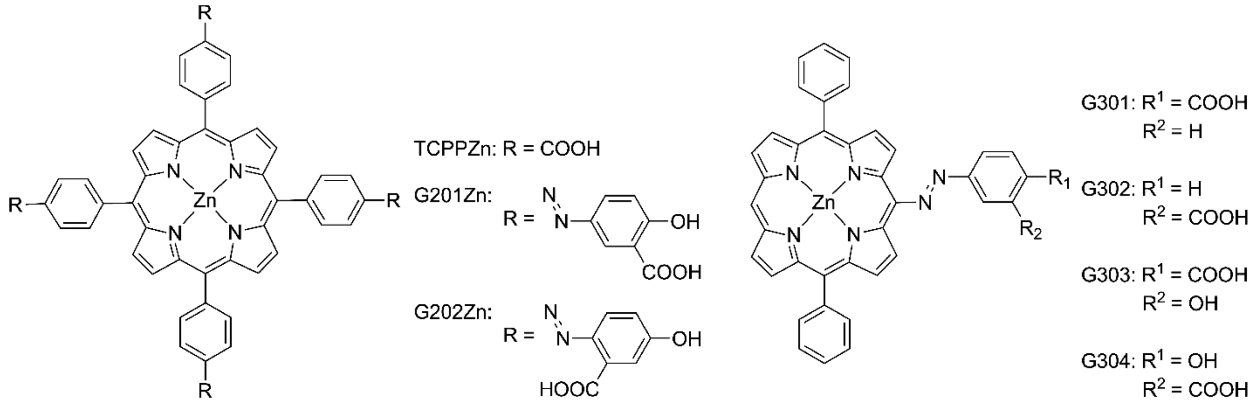

Figure 1. Structure of zinc porphyrin dyes.

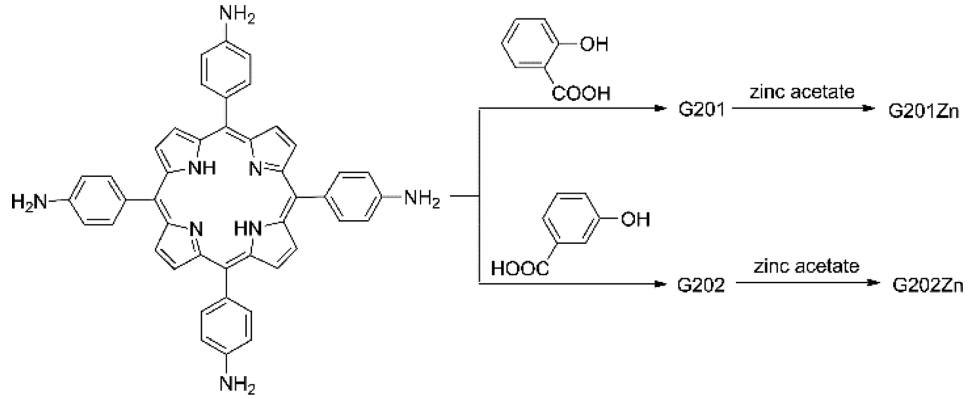

Figure 2. Synthetic protocol for G2 series dyes.

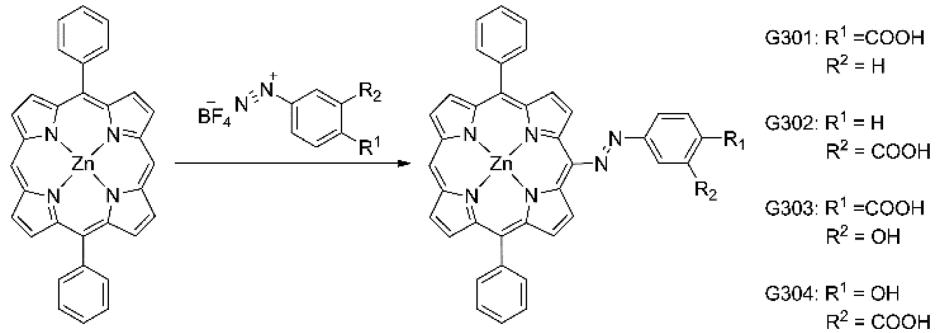

Figure 3. Synthetic protocol for G3 series dyes.

further extend and verify the effect of salicylic acid as an anchoring group, we also designed and synthesized *meso-azo*-bridged zinc porphyin dyes of G301, G302, G303, and G304 (Figure 1) using a new protocol to approach (Figure 3). To demonstrate the impacts of a new anchoring group of salicylic acid and a new π-conjugated bridge of the *azo* group, the detailed investigations of the new dyes and the performances of their DSSC devices were carried out in comparison to those of DSSCs using N719 and TCPPZn as sensitizers.

EXPERIMENTAL SECTION

General. All solvents were treated by standard methods prior to use. 1,2-Dimethyl-3-propylimidazolium iodide (DMPII) was purchased from TCI, and 4-*tert*-butylpyridine and iodine were purchased from Aldrich and used without further purification. All other chemicals were analytical grade and used as received. FTO glass was purchased from Nippon Sheet Glass Co. Ltd. (15 Ω/cm^2). The NMR spectra were recorded on a Varian Mercury 300 spectrometer or on a Bruker AVANCE III 400 spectrometer using tetramethylsilane (TMS) as the internal standard. The MALDI-TOF mass spectra were acquired by a Bruker BIFLEX III spectrometer workstation. The ESI mass spectra were acquired by a Bruker ESQUIRE 6000 spectrometer. The UV−vis absorption spectra were determined by an UV-3600 spectrophotometer in DMSO:EtOH = 10:1 (G201Zn, G202Zn, TCPPZn) or THF (G301, G302, G303, G304) at room temperature. The fluorescence spectra were obtained by a F-7000 fluorescence spectrophotometer with a Xe lamp as light source.

Synthesis and Characterization. General Procedure for Free Base Porphyrins G201 and G202. 5,10,15,20-*tetra*-(*p*-Ammiophenyl) porphyrin (TAPP) (0.335 g, 0.5 mmol) was added to a hydrochloric acid solution (1.2 M, 10 mL) under vigorous stirring in an ice−water bath for 30 min. When the mixture was cooled to 0−5 °C, a solution of $NaNO_2$ (0.140 g, 2 mL) was added dropwise and stirred for 1 h. Then, a solution of the hydroxybenzoic acid (0.276 g, 2 mmol) dissolved in 10% NaOH solution (5 mL) was added dropwise to the reaction mixture and kept vigorous stirring for 12 h at 0−5 °C.

The resulting mixture was acidified with 10% acetic acid solution to generate green precipitate that was filtered, washed with water, and dried in air. The crude product was recrystallized from DMF to yield pure free base porphyrin of G201 or G202 (93%−96%).

G201. ^{1}H NMR (300 MHz, DMSO-d_6) δ 12.80 (4H, br, COOH), 8.87 (8H, s, ß-pyrrole), 8.45 (4H, s, Ar−H), 8.32−8.15 (20H, m, Ar−H, ß-pyrrole), 7.16 (4H, d, J = 9.3 Hz, Ar−H), 3.45 (4H, br, OH), 2.90 (2H, s, N−H). ^{13}C NMR (101 MHz, DMSO-d_6) δ 171.8, 164.2, 151.6, 145.0, 144.0, 135.7, 129.3, 126.5, 121.3, 118.8, 114.2. MS (MALDI-TOF): calc. for $C_{72}H_{46}N_{12}O_{12}$, m/z: 1271.2; found: 1272.0 $(M+H)^+$.

G202. ^{1}H NMR (300 MHz, DMSO-d_6) δ 10.66 (4H, br, COOH), 8.89 (8H, s, ß-pyrrole), 8.45 (8H, d, J = 8.1 Hz, Ar−H), 8.24 (8H, d, J = 8.1 Hz, Ar−H), 7.85 (4H, d, J = 9.0 Hz, Ar−H), 7.16 (4H, d, J = 2.4 Hz, Ar−H), 7.12 (4H, dd, J = 2.4, 9.0 Hz, Ar−H), 3.67 (4H, b, OH), 2.82 (2H, s, N−H). ^{13}C NMR (101 MHz, DMSO-d_6) δ 169.1, 161.0, 152.1, 144.1, 143.1, 135.9, 135.5, 121.5, 120.0, 118.5, 115.2, MS (ESI): calc. for $C_{72}H_{46}N_{12}O_{12}$, m/z: 1271.2; found: 1272.7 $(M+H)^+$.

General Procedure for *azo*-Bridged Zinc Porphyrin Dyes G201Zn and G202Zn. Zinc acetate dihydrate (0.438 g) was added to a DMF solution (100 mL) dissolved free base porphyrin (0.480 g) that was heated to reflux for 12 h. Then, 200 mL of water was added to quench the reaction allowing the purple precipitate formed. The obtained purple crystals was filtered and washed with water for many times to give our target dye of G201Zn or G202Zn.

G201Zn. ^{1}H NMR (300 MHz, DMSO-d_6) 12.0 (4H, br, COOH), 8.92 (8H, s, ß-pyrrole), 8.48 (4H, d, J = 2.7 Hz, Ar−H), 8.36 (8H, d, J = 8.1 Hz, Ar−H), 8.23 (8H, d, J = 8.1 Hz, Ar−H), 8.02 (4H, dd, J = 2.7, 8.7 Hz, Ar−H), 6.92 (4H, d, J = 8.7 Hz, Ar−H). ^{13}C NMR (101 MHz, DMSO-d_6) δ 172.1, 167.7, 151.8, 149.7, 145.1, 143.9, 135.7, 132.4, 128.0, 126.6, 120.8, 118.4. MS (MALDI-TOF): calc. for $C_{72}H_{44}N_{12}O_{12}Zn$: m/z 1334.6; found: 1334.9 $(M)^+$.

G202Zn. ^{1}H NMR (300 MHz, DMSO-d_6) δ 10.63 (4H, br, COOH), 10.40 (4H, br, OH), 8.99 (8H, s, ß-pyrrole), 8.38−8.21 (16H, m, Ar−H), 7.83 (4H, Ar−H), 7.13 (8H, Ar−H). ^{13}C NMR (101 MHz; DMSO-d_6) δ 160.8, 151.7, 149.7, 145.6, 143.0, 13.6, 132.3, 121.2, 120.2, 119.8, 118.1, 115.1. MS (MALDI-TOF): calc. for $C_{72}H_{44}N_{12}O_{12}Zn$: m/z 1334.6; found: 1334.9 $(M)^+$.

General Procedure for *meso-azo*-Bridged Zinc Porphyin Dyes G301, G302, G303, and G304. A methanol solution (50 mL) of diazonium tetrafluoroborate (0.325 g) was added dropwise to a THF solution (100 mL) of 10,20-biphenylporphinato zinc(II) (0.135 g) under stirring at 0−5 °C for 15 h. The resulting mixture was then passed through a short silica plug. After evaporating the solvents, the residue was chromatographed on silica eluting with CH_2Cl_2-methanol and crystallized from CH_2Cl_2 to yield porphyin dye as green crystals (40−60%).

G301. ^{1}H NMR (400 MHz; DMSO-d_6) δ 12.93 (1H, br, COOH), 10.32 (1H, s, *meso*-H), 9.88 (2 H, d, J = 4.7 Hz, ß-pyrrole), 9.41 (2 H, d, J = 4.4 Hz, ß-pyrrole), 8.88 (2 H, d, J = 4.7 Hz, ß-pyrrole), 8.76 (2 H, d, J = 4.4 Hz, ß-pyrrole), 8.51 (2 H, d, J = 8.4 Hz, azoAr−H), 8.36 (2 H, d, J = 8.4 Hz, azoAr−H), 8.20 (4 H, m, Ar−H), 7.85 (6H, Ar−H). ^{13}C NMR (101 MHz; DMSO-d_6) δ 168.69, 156.06, 150.95, 149.45, 149.36, 147.39, 142.61, 134.57, 133.46, 133.29, 132.07, 131.28, 131.13, 128.73, 128.23, 127.32, 123.02, 122.62, 110.64. MS (MALDI-TOF): calc. for $C_{39}H_{24}N_6O_2Zn$: m/z 674.0; found: 673.1 $(M-1)^+$.

G302. ^{1}H NMR (400 MHz; DMSO-d_6) δ 13.40 (1H, br, COOH), 10.34 (1H, s, *meso*-H), 9.86 (2 H, d, J = 4.7 Hz, ß-pyrrole), 9.43 (2 H, d, J = 4.5 Hz, ß-pyrrole), 8.94 (1 H, s, azoAr−H), 8.89 (2 H, d, J = 4.7 Hz, ß-pyrrole), 8.78 (2 H, d, J = 4.5 Hz, ß-pyrrole), 8.71 (1 H, d, J = 7.7 Hz, azoAr−H), 8.26 (1H, d, J = 7.7 Hz, azoAr−H), 8.21 (4 H, m, Ar−H), 7.95 (1 H, t, J = 7.7 Hz, azoAr−H), 7.86 (6H, Ar−H). ^{13}C NMR (101 MHz; DMSO-d_6) δ 169.03, 154.41, 150.84, 149.47, 149.38, 147.16, 142.62, 134.59, 133.48, 133.29, 132.12, 131.60, 130.99, 130.66, 128.66, 128.23, 127.31, 123.86, 122.89, 110.38, 107.48, 97.60. MS (MALDI-TOF): calc. for $C_{39}H_{24}N_6O_2Zn$: m/z 674.0; found: 673.1 $(M-1)^+$.

G303. ^{1}H NMR (400 MHz; DMSO-d_6) δ 17.73 (1H, br, COOH), 10.26 (1H, s, *meso*-H), 9.71 (2 H, d, J = 4.7 Hz, ß-pyrrole), 9.41 (2 H, d, J = 4.5 Hz, ß-pyrrole), 8.86 (2 H, d, J = 4.7 Hz, ß-pyrrole), 8.81 (1H, s, azoAr−H), 8.80 (2H, d, J = 4.5 Hz, ß-pyrrole), 8.42 (1H, dd, J = 8.7 Hz, 2.7 Hz, azoAr−H), 8.21 (4 H, m, Ar−H), 7.85 (6H, Ar−H), 7.53 (1H, br, OH), 7.04 (1H, d, J = 8.7 Hz, azoAr−H). ^{13}C NMR (101 MHz; DMSO-d_6) δ171.58, 150.21, 149.69, 149.22, 146.14, 145.95, 142.93, 134.66, 132.81, 132.53, 132.15, 131.07, 130.64, 128.07, 127.59, 127.25, 126.24, 121.65, 119.94, 118.46, 108.16, 97.59. MS (MALDI-TOF): calc. for $C_{39}H_{24}N_6O_3Zn$: m/z 690.0; found: 689.1 $(M-1)^+$.

G304. ^{1}H NMR (400 MHz; DMSO-d_6) δ 16.69 (1H, br, COOH), 15.78 (1H, br, OH), 10.32 (1H, s, *meso*-H), 9.81 (2 H, d, J = 4.7 Hz, ß-pyrrole), 9.42 (2 H, d, J = 4.4 Hz, ß-pyrrole), 8.88 (2 H, d, J = 4.7 Hz, ß-pyrrole), 8.78 (2H, d, J = 4.4 Hz, ß-pyrrole), 8.21 (4 H, m, Ar−H), 8.12 (1H, d, J = 8.1 Hz, azoAr−H), 7.85 (6H, Ar−H), 7.77 (1H, dd, J = 8.1 Hz, 1.9 mHz, azoAr−H), 7.69 (1H, d, J = 1.9 Hz, azoAr−H). ^{13}C NMR (101 MHz; DMSO-d_6) δ171.73, 156.90, 150.71, 149.48, 149.35, 146.86, 142.71, 134.60, 133.25, 133.15, 132.09, 131.55, 130.98, 129.19, 128.18, 127.29, 122.53, 111.77, 109.57, 104.39, 100.99, 97.63. MS (MALDI-TOF): calc. for $C_{39}H_{24}N_6O_3Zn$: m/z 690.0; found: 689.1 $(M-1)^+$

TCPPZn were prepared following the literature method.[18]

Preparation of Photovoltaic Cells. The usable TiO_2 paste containing polyethylene glycol (molecular weight 20000) in a proportion of 50% weight was coated on a commercial fluorine−tin-oxide (FTO) using vacuum spincoater method. The FTO glass supported TiO_2 film (thickness 15 μm and active area 0.16 cm^2) was then sintered at 500 °C for 1 h. After the oven temperature was cooled to 100 °C, the electrode was immerged immediately into the dye solution (G2 series, 1 mM, DMSO, 120 h; G3 series, 0.5 mM, EtOH/toluene = 1/1, 12 h). The TiO_2 electrode was then taken out, flushed with CH_3CN, and dried with nitrogen stream. The solar cell was prepared by agglutinating the platinum counter electrode and the TiO_2 electrode. Electrolyte was injected and penetrated to the TiO_2 film *via* vacuum perfusion. The electrolyte solution was constitutive of 0.6 M DMPII, 0.05 M I_2, and 0.5 M TBP in a mixture solution of acetonitrile and valeronitrile (85:15, v/v). The solar cell was finally sealed by hot glue.

Photoelectrochemistry and Electrochemistry. The detailed dye-loading examination was presented in the SI. The performances of device were recorded through measurement of (J-V) curves on a Keithley 2601A Source Meter with an AM-1.5 G solar simulator (San-Ei XES-301S). The incident light intensity was 100 mW/cm^2 calibrated with a standard Si solar cell. The incident photon-to-current conversion efficiency (IPCE) of the corresponding devices was measured with a Crown instrument. Cyclic voltammetry curves were obtained by a CHI 660D potentiostat instrument with a traditional three-electrode system. The working electrode, reference electrode, and auxiliary electrode was a glassy carbon disk electrode, Ag/Ag$^+$ and Pt-wire electrode, respectively. The electrochemical impedance spectroscopy (EIS) was carried out on a Zahner impedance analyzer (IM6ex) controlled by a computer with Thales software. The frequency of the AC signal ranged between 100 mHz and 1 MHz. The amplitude of the AC signal was 10 mV at room temperature.

RESULTS AND DISCUSSION

Photophysical and Electrochemical Properties. The UV−vis spectra of the G201Zn, G202Zn, and TCPPZn were shown in Figure 4. The peak positions and molar absorption coefficients as well as the emission wavelengths were listed in Table 1. The *azo* structure showed short-wavelength peaks at 357 nm for G201Zn and 358 nm for G201Zn. The elongation of the π-conjugation made their Soret and Q bands become broader and shift toward longer wavelengths compared with TCPPZn.[29] The electrochemical properties of the dyes were measured by cyclic voltammetry and presented in Table 1. The ground-state oxidation potentials (E_{ox}) of dyes were +0.84 V for G201Zn and +0.90 V for G202Zn, that were far below the redox potential of I^-/I_3^- (0.4 V) to ensure efficient regeneration. The excitation energies (E_{0-0}) were determined to be 2.05 eV for G201Zn and 2.03 eV for G202Zn, respectively. The injection potentials ($E_{S+/S*}$) subtracted the

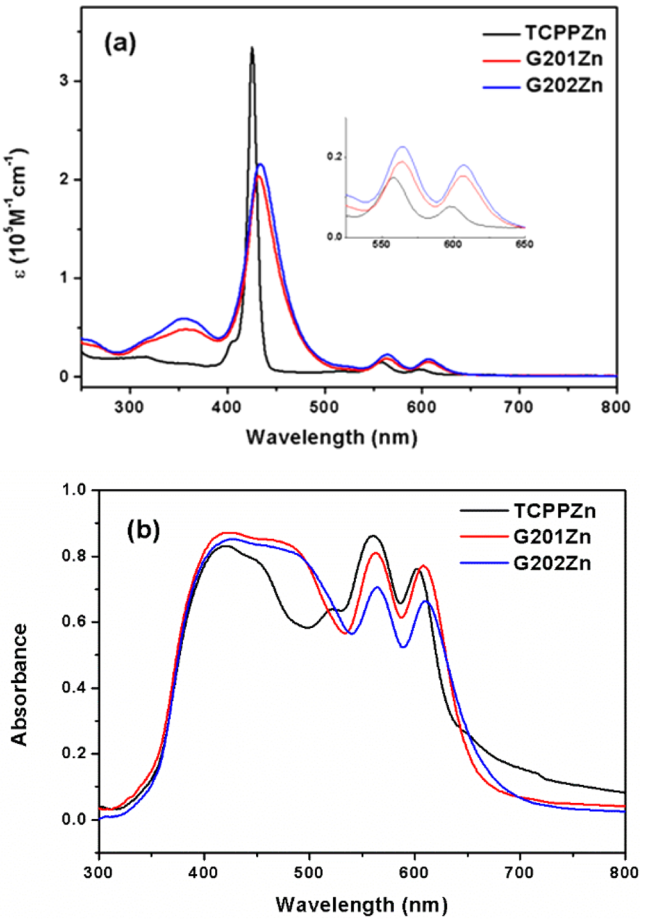

Figure 4. (a) UV/vis absorption spectra of G2 series dyes in EtOH/DMSO (10:1). (b) UV/vis absorption spectra of zinc porphyrin dyes on TiO_2 film.

Table 1. Absorption/Emission and Electrochemical Properties of G2 Series Dyes

dye	absorption λ_{max}[a] (nm) (ε[10^3 M^{-1} cm^{-1}])	emission λ_{max}[a] (nm)	E_{OX}[b] (V vs NHE)	E_{S+/S^*}[c] (V)	E_{0-0}[d] (V vs NHE)
TCPPZn	425(334), 558(14.9), 597(7.8)	612	1.04	−1.08	2.12
G202Zn	358(18.0), 433(216), 565(22.7), 607(18.0)	625	0.90	−1.13	2.03
G201Zn	357(15.3), 432(204), 564(18.9), 606(15.3)	624	0.84	−1.21	2.05

[a]Absorption and emission spectra were measured in EtOH/DMSO (10:1) solution. [b]The oxidation potentials of dyes were measured in DMSO with 0.1 M tetrabutylammonium hexafluorophosphate ($TBAPF_6$) with a scan rate of 50 mVs^{-1} (vs NHE). [c]E_{S+/S^*} was calculated by $E_{ox} - E_{0-0}$. [d]E_{0-0} was determined from the intersection of normalized absorption and emission spectra.

E_{0-0} from the E_{ox} of the sensitizers was much higher than the potential of the conducting band of TiO_2 nanoparticles (0.5 V).[30]

FTIR spectra of the pure dye and the dyes adsorbed on TiO_2-nanoparticles have been measured respectively to explore the anchoring modes for G201Zn and G202Zn (Supporting Information, Figure S2). The IR spectrum of TCPPZn displayed a strong band in the region of 1685−1695 cm^{-1} attributed to the $\nu_{C=O}$ stretch vibration and a broad band at 1270−1285 cm^{-1} attributed to the ν_{C-O} stretch vibration of the carboxylic acid groups. The hydrogen bonding of the carboxyl and hydroxyl groups in G201Zn resulted in a red-shift to lower frequency of the $\nu_{C=O}$ stretch vibration at 1648 cm^{-1} and a blue-shift to higher frequency of the ν_{C-O} stretch vibration at 1382 cm^{-1}, respectively. When the dyes were adsorbed on the TiO_2 surface, the $\nu_{C=O}$ stretch vibration of the carboxylic acid groups disappeared with the appearance of a broad shoulder on the high-frequency side of the phenyl breathing vibration (1580−1620 cm^{-1}). Furthermore, a broad band observed at 1382 cm^{-1} for G201Zn also disappeared, which might be attributed to the binding modes between salicylic acid and TiO_2 nanoparticles.

DFT Calculations and Energy Levels. Geometries and energies of the stationary points found herein were fully optimized by hybrid density functional theory (DFT) using the GAUSSIAN 09 program suite.[31] For our calculations, the hybrid gradient corrected exchange functional of B3LYP was used.[32,33] The standardized 6-31G basis set was used together with the polarization (d) functions basis set[34,35] for all atoms except Zn that was depicted by the effective core potential LANL2DZ basis set.[36,37] The MO patterns of HOMO and LUMO of zinc porphyrin dyes were shown in Figure 5. Our

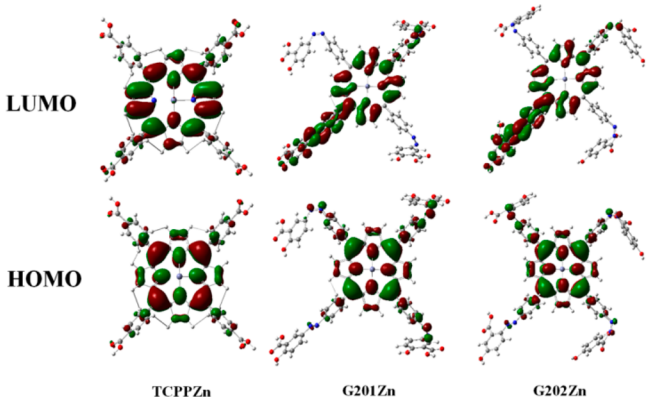

Figure 5. Molecular orbitals of TCPPZn, G201Zn, and G202Zn.

DFT calculations demonstrated that when the nitrogen−nitrogen double bonds were stayed at *trans* configuration, electrons in the frontier molecular orbital delocalized from the zinc porphyrin ring to the *azo* bridge, π system, and the salicylic acid group. Figure 6 displays that the energy level of conducting

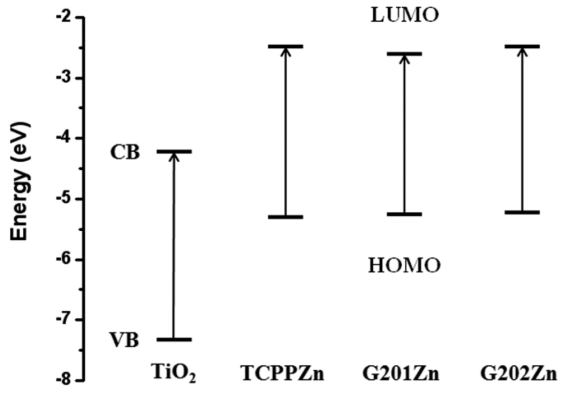

Figure 6. Energy-level diagram of zinc porphyrin dyes and anatase TiO_2.

band of TiO_2 is located between that of the LUMO and the HOMO of zinc porphyrin dyes. These results confirm that the electron injection from the LUMO of dyes to the conducting band of TiO_2 is quite available.

Photovoltaic Performance of DSSCs. The current density−voltage (*J-V*) curves of DSSCs with G201Zn, G202Zn, and TCPPZn were shown in Figure 7. The

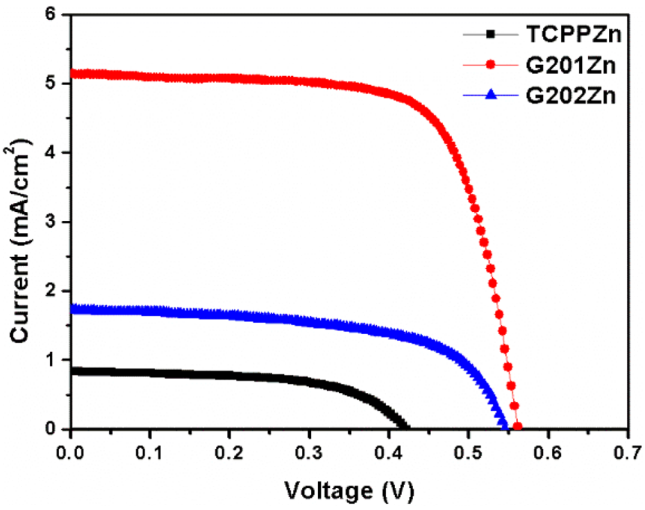

Figure 7. *J*-V characteristics of DSSCs sensitized with G2 series dyes.

Table 2. Photovoltaic Performance of Dye Sensitized Solar Cells Based on G2 Series Dyes

dye	V_{oc} (V)	Jsc (mA/cm^2)	FF (%)	η (%)
TCPPZn	0.42	0.84	57.9	0.20
G202Zn	0.55	1.73	59.5	0.56
G201Zn	0.56	5.14	70.8	2.04
N719	0.75	13.31	64.1	6.39

photovoltaic parameters were listed in Table 2. The common efficiency of the DSSCs sensitized by TCPPZn is around 0.1%,[9,16] whereas the cell performance of G201Zn and G202Zn demonstrated respectively 2.04% and 0.56% photoelectronic conversion efficiency. These higher efficiencies than that of TCPPZn indicate the *azo* structure is a successful bridge. The open-circuit voltages of the cells sensitized by G201Zn and G202Zn reached 0.55 V, which were higher than that of TCPPZn. As for J_{SC}, the values displayed were 5.14 mA/cm^2 for G201Zn and 1.73 mA/cm^2 for G202Zn, respectively. The performance of G201Zn sensitized solar cells was even better than that of G202Zn. The reason would be attributed to the *ortho* position between the hydroxyl group and the carboxyl group in the salicylic acid.

The incident photon to current conversion efficiency (IPCE) spectra of the solar cells were depicted in Figure 8. G201Zn and G202Zn demonstrated an obvious enhancement and red-shift to IPCE compared with TCPPZn. This effect might be attributed to the efficient interfacial quantum yields of electron injection from the dye to the TiO_2 surface. It can be seen that when the carboxyl and hydroxyl group in G201Zn is located in the *meta* and *para* positions of *azo* bridge, respectively, both of them would anchor to the surface of TiO_2 *via* a tridentate binding mode (Figure 9) that is favor to the electron

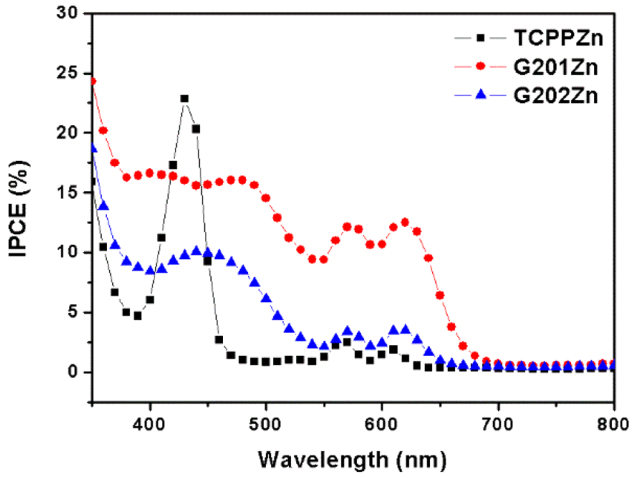

Figure 8. IPCE of DSSCs sensitized with G2 series dyes.

transportation.[38] In contrast, the carboxyl group of G202Zn lies at the *ortho* position of the *azo* group, the hydroxyl is highly hindered to bind onto the TiO_2 surface because of the steric clashes at the periphery of the rigid flat, and this leads to a bidentate binding mode.

Electrochemical Impedance Spectroscopy. The interfacial charge transfer in DSSCs was measured by electrochemical impedance spectroscopy (EIS) under dark conditions at a forward bias of −0.6 V.[39,40] The Nyquist and Bode plots are shown in Figure 10. Nyquist plots have three semicircles, and the larger semicircle at intermediate frequencies represents the interfacial charge transfer resistance (R_{ct}) at the TiO_2/dye/electrolyte interface. The fitted R_{ct} values of G201Zn-based devices are much larger than those of other devices. This indicates that the recombination rate of electrons from the conducting band to the electrolyte increased in the following order: G201Zn < G202Zn < TCPPZn. The larger the R_{ct} value, the more difficult the electrons recombination. As a result, both J_{sc} and V_{oc} increased in the solar cell sensitized by G201Zn.[41,42] In the Bode phase plot, the G201Zn-based devices showed a lower frequency peak than that of G202Zn and TCPPZn based devices, which indicated that they had a longer electron lifetime. Their different electrochemical impedance spectroscopy implied that the salicylic structure as an anchoring group could promote charge injection efficiency due to its intimate contact with the semiconductor surface *via* a tridentate binding mode.

To further verify the tridentate binding mode, the performances of the G3 series dyes were investigated by photophysical and photovoltaic methods (Supporting Information), and the photovoltaic parameters were collected and displayed in Table 3. The cell performance of G304 demonstrated almost four times photoelectric conversion efficiency than that of G301, G302, and G303 owing to tridentate binding mode of G304 vs the bidentate binding modes of G301, G302, and G303. We must emphasize that the carboxyl group and hydroxyl group were respectively located in the *meta* position and the *para* position of *azo*-bridged benzene ring in G304 as well as in G201; this configuration allows it to anchor to the TiO_2 surface with the tridentate binding mode leading to higher electron injection efficiency. In contrast, when the carboxyl group and the hydroxyl group were respectively located in the *para* position and the *meta* position of *azo*-bridged benzene ring in

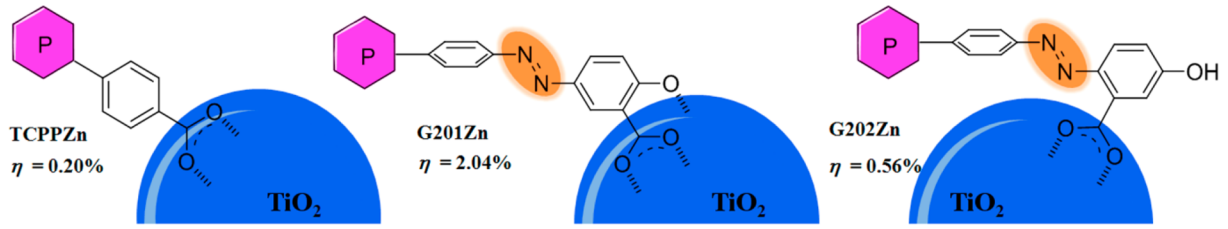

Figure 9. The sketch map of binding modes.

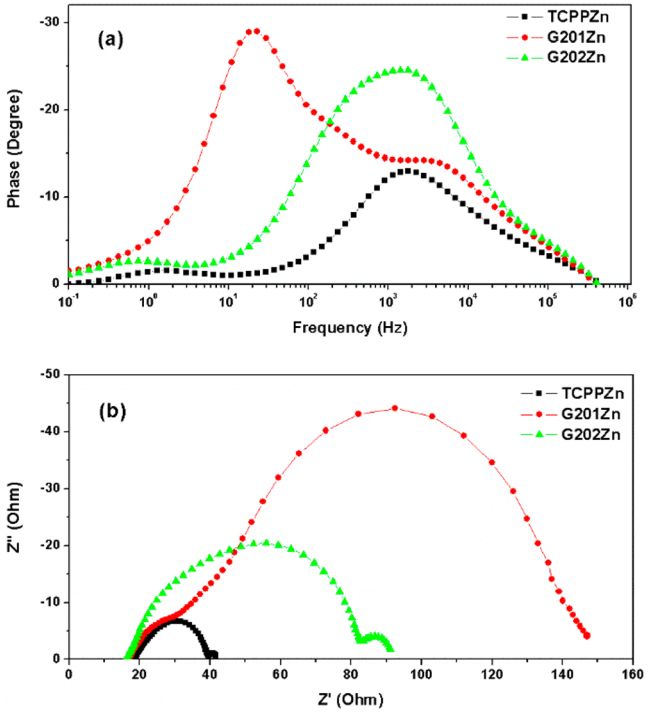

Figure 10. EIS spectra of DSSCs based on G2 series dyes coadsorbent measured at −0.60 V forward bias in the dark: (a) Bode phase plots and (b) Nyquist diagram.

Table 3. Photovoltaic Performance of Dye Sensitized Solar Cells Based on G3 Series Dyes

dye	V_{oc} (V)	Jsc (mA/cm^2)	FF (%)	η (%)
G301	0.45	0.56	44.9	0.11
G302	0.45	0.50	44.8	0.10
G303	0.46	0.60	46.4	0.13
G304	0.44	1.79	44.8	0.35

G303, the binding mode is still bidentate due to the space effect leading to lower electron injection efficiency.

CONCLUSION

Two series dyes of *azo*-bridged zinc porphyrins using carboxyl and hydroxyl as anchoring groups have been designed and synthesized. The *azo* group could be used successfully as a conjugated bridge in sensitizers. The photoelectric conversion efficiency of the G201Zn-sensitized solar cells is ten times higher than that of TCPPZn. The tridentate binding modes between salicylic acid and TiO_2 nanoparticles should enhance the interfacial quantum yields of electron injection. This idea might be expanded to other dyes. We are currently working toward this direction, and the results will be reported in due course.

ASSOCIATED CONTENT

Supporting Information

The FTIR, UV−vis, and more calculation results. This material is available free of charge via the Internet at http://pubs.acs.org.

AUTHOR INFORMATION

Corresponding Author

*Phone: 86-931-8912585. Fax: 86-931-8912582. E-mail: hwjing@lzu.edu.cn.

Notes

The authors declare no competing financial interest.

ACKNOWLEDGMENTS

The authors gratefully acknowledge Prof. Ran Fang for the DFT Calculations. The authors acknowledge the financial support of this work from the National Natural Science Foundation of China (NSFC 21173106) and by the Foundation of State Key Laboratory of Coal Conversion (Grant No. J12-13-901).

REFERENCES

(1) O'Regan, B.; Grätzel, M. *Nature* **1991**, *353*, 737−740.
(2) Hagfeldt, A.; Boschloo, G.; Sun, L.; Kloo, L.; Pettersson, H. *Chem. Rev.* **2010**, *110*, 6595−6663.
(3) Hardin, B. E.; Snaith, H. J.; McGehee, M. D. *Nat. Photonics* **2012**, *6*, 162−169.
(4) Ning, Z.; Fu, Y.; Tian, H. *Energy Environ. Sci.* **2010**, *3*, 1170−1181.
(5) Nazeeruddin, M. K.; Kay, A.; Rodicio, I.; Humphry-Baker, R.; Mueller, E.; Liska, P.; Vlachopoulos, N.; Grätzel, M. *J. Am. Chem. Soc.* **1993**, *115*, 6382−6390.
(6) Nazeeruddin, M. K.; De Angelis, F.; Fantacci, S.; Selloni, A.; Viscardi, G.; Liska, P.; Ito, S.; Takeru, B.; Grätzel, M. *J. Am. Chem. Soc.* **2005**, *127*, 16835−16847.
(7) Yu, Q.; Wang, Y.; Yi, Z.; Zu, N.; Zhang, J.; Zhang, M.; Wang, P. *ACS Nano* **2010**, *4*, 6032−6038.
(8) Li, L. L.; Diau, E. W. G. *Chem. Soc. Rev.* **2013**, *42*, 291−304.
(9) Campbell, W. M.; Burrell, A. K.; Officer, D. L.; Jolley, K. W. *Coord. Chem. Rev.* **2004**, *248*, 1363−1379.
(10) Odobel, F.; Blart, E.; Lagree, M.; Villieras, M.; Boujtita, H.; El Murr, N.; Caramori, S.; Alberto Bignozzi, C. *J. Mater. Chem.* **2003**, *13*, 502−510.
(11) Hart, A. S.; KC, C. B.; Gobeze, H. B.; Sequeira, L. R.; D'Souza, F. *ACS Appl. Mater. Interfaces* **2013**, *5*, 5314−5323.
(12) Lee, C. W.; Lu, H. P.; Lan, C. M.; Huang, Y. L.; Liang, Y. R.; Yen, W. N.; Liu, Y. C.; Lin, Y. S.; Diau, E. W. G.; Yeh, C. Y. *Chem.—Eur. J.* **2009**, *15*, 1403−1412.
(13) Ripolles-Sanchis, T.; Guo, B. C.; Wu, H. P.; Pan, T. Y.; Lee, H. W.; Raga, S. R.; Fabregat-Santiago, F.; Bisquert, J.; Yeh, C. Y.; Diau, E. W. G. *Chem. Commun.* **2012**, *48*, 4368−4370.
(14) Chang, Y. C.; Wang, C. L.; Pan, T. Y.; Hong, S. H.; Lan, C. M.; Kuo, H. H.; Lo, C. F.; Hsu, H. Y.; Lin, C. Y.; Diau, E. W. G. *Chem. Commun.* **2011**, *47*, 8910−8912.

(15) Wang, C. L.; Lan, C. M.; Hong, S. H.; Wang, Y. F.; Pan, T. Y.; Chang, C. W.; Kuo, H. H.; Kuo, M. Y.; Diau, E. W. G.; Lin, C. Y. *Energy Environ. Sci* **2012**, *5*, 6933−6940.
(16) Yella, A.; Lee, H.-W.; Tsao, H. N.; Yi, C.; Chandiran, A. K.; Nazeeruddin, M. K.; Diau, E. W.-G.; Yeh, C.-Y.; Zakeeruddin, S. M.; Grätzel, M. *Science* **2011**, *334*, 629−634.
(17) Rochford, J.; Chu, D.; Hagfeldt, A.; Galoppini, E. *J. Am. Chem. Soc.* **2007**, *129*, 4655−4665.
(18) Li, B.; Chen, J.; Zheng, J.; Zhao, J.; Zhu, Z.; Jing, H. *Electrochim. Acta* **2012**, *59*, 207−212.
(19) Galoppini, E. *Coord. Chem. Rev.* **2004**, *248*, 1283−1297.
(20) O'Regan, B.; Xiaoe, L.; Ghaddar, T. *Energy Environ. Sci.* **2012**, *5*, 7203−7215.
(21) Ooyama, Y.; Harima, Y. *ChemPhysChem* **2012**, *13*, 4032−4080.
(22) Tae, E. L.; Lee, S. H.; Lee, J. K.; Yoo, S. S.; Kang, E. J.; Yoon, K. B. *J. Phys. Chem. B* **2005**, *109*, 22513−22522.
(23) He, H.; Gurung, A.; Si, L. *Chem. Commun.* **2012**, *48*, 5910−5912.
(24) Jiao, C.; Zu, N.; Huang, K. W.; Wang, P.; Wu, J. *Org. Lett.* **2011**, *13*, 3652−3655.
(25) Ooyama, Y.; Nagano, T.; Inoue, S.; Imae, I.; Komaguchi, K.; Ohshita, J.; Harima, Y. *Chem.—Eur. J.* **2011**, *17*, 14837−14843.
(26) Mao, J.; He, N.; Ning, Z.; Zhang, Q.; Guo, F.; Chen, L.; Wu, W.; Hua, J.; Tian, H. *Angew. Chem., Int. Ed.* **2012**, *51*, 9873−9876.
(27) Zhao, J.; Yang, X.; Cheng, M.; Li, S.; Sun, L. *ACS Appl. Mater. Interfaces* **2013**, *5*, 5227−5231.
(28) Mikroyannidis, J. A.; Tsagkournos, D. V.; Balraju, P.; Sharma, G. D. *J. Power Sources* **2011**, *196*, 4152−4161.
(29) Imahori, H.; Umeyama, T.; Ito, S. *Acc. Chem. Res.* **2009**, *42*, 1809−1818.
(30) Kang, M. S.; Kang, S. H.; Kim, S. G.; Choi, I. T.; Ryu, J. H.; Ju, M. J.; Cho, D.; Lee, J. Y.; Kim, H. K. *Chem. Commun.* **2012**, *48*, 9349−9351.
(31) Frisch, M. J.; Trucks, G. W.; Schlegel, H. B.; Scuseria, G. E.; Robb, M. A.; Cheeseman, J. R.; Scalmani, G.; Barone, V.; Mennucci, B.; Petersson, G. A.; Nakatsuji, H.; Caricato, M.; Li, X.; Hratchian, H. P.; Izmaylov, A. F.; Bloino, J.; Zheng, G.; Sonnenberg, J. L.; Hada, M.; Ehara, M.; Toyota, K.; Fukuda, R.; Hasegawa, J.; Ishida, M.; Nakajima, T.; Honda, Y.; Kitao, O.; Nakai, H.; Vreven, T.; Montgomery, J. A., Jr.; Peralta, J. E.; Ogliaro, F.; Bearpark, M.; Heyd, J. J.; Brothers, E.; Kudin, K. N.; Staroverov, V. N.; Kobayashi, R.; Normand, J.; Raghavachari, K.; Rendell, A.; Burant, J. C.; Iyengar, S. S.; Tomasi, J.; Cossi, M.; Rega, N.; Millam, N. J.; Klene, M.; Knox, J. E.; Cross, J. B.; Bakken, V.; Adamo, C.; Jaramillo, J.; Gomperts, R.; Stratmann, R. E.; Yazyev, O.; Austin, A. J.; Cammi, R.; Pomelli, C.; Ochterski, J. W.; Martin, R. L.; Morokuma, K.; Zakrzewski, V. G.; Voth, G. A.; Salvador, P.; Dannenberg, J. J.; Dapprich, S.; Daniels, A. D.; Farkas, Ö.; Foresman, J. B.; Ortiz, J. V.; Cioslowski, J.; Fox, D. J. *Gaussian 09, Revision A.01*; Gaussian, Inc.: Wallingford, CT, 2009.
(32) Becke, A. D. *J. Chem. Phys.* **1993**, *98*, 5648−5652.
(33) Lee, C.; Yang, W.; Parr, R. G. *Phys. Rev. B* **1988**, *37*, 785−789.
(34) Rassolov, V. A.; Ratner, M. A.; Pople, J. A.; Redfern, P. C.; Curtiss, L. A. *J. Comput. Chem.* **2001**, *22*, 976−984.
(35) Rassolov, V. A.; Pople, J. A.; Ratner, M. A.; Windus, T. L. *J. Chem. Phys.* **1998**, *109*, 1223−1229.
(36) Hay, P. J.; Wadt, W. R. *J. Chem. Phys.* **1985**, *82*, 270−283.
(37) Wadt, W. R.; Hay, P. J. *J. Chem. Phys.* **1985**, *82*, 284−298.
(38) Nazeeruddin, M. K.; Humphry-Baker, R.; Liska, P.; Grätzel, M. *J. Phys. Chem. B* **2003**, *107*, 8981−8987.
(39) Wang, Q.; Moser, J.-E.; Grätzel, M. *J. Phys. Chem. B* **2005**, *109*, 14945−14953.
(40) Fabregat-Santiago, F.; Garcia-Belmonte, G.; Mora-Sero, I.; Bisquert, J. *Phys. Chem. Chem. Phys.* **2011**, *13*, 9083−9118.
(41) Song, B. J.; Song, H. M.; Choi, I. T.; Kim, S. K.; Seo, K. D.; Kang, M. S.; Lee, M. J.; Cho, D. W.; Ju, M. J.; Kim, H. K. *Chem.—Eur. J.* **2011**, *17*, 11115−11121.
(42) Song, H. M.; Seo, K. D.; Kang, M. S.; Choi, I. T.; Kim, S. K.; Eom, Y. K.; Ryu, J. H.; Ju, M. J.; Kim, H. K. *J. Mater. Chem.* **2012**, *22*, 3786−3794.